JBC EDITORS' PICK

Cation channel conductance and pH gating of the innate immunity factor APOL1 are governed by pore-lining residues within the C-terminal domain

Received for publication, May 4, 2020, and in revised form, July 24, 2020 Published, Papers in Press, July 29, 2020, DOI 10.1074/jbc.RA120.014201

Charles Schaub[1,2], **Joseph Verdi**[1,3,4], **Penny Lee**[1], **Nada Terra**[1], **Gina Limon**[1,5], **Jayne Raper**[1], **and Russell Thomson**[1,*]

From the [1]Department of Biological Sciences, Hunter College, CUNY, New York, New York, USA, the [2]Program in Biochemistry, the [3]Program in Biology, The Graduate Center, CUNY, New York, New York, USA, the [4]German Cancer Research Center, Heidelberg, Germany, and the [5]NYU School of Medicine, New York, New York, USA

Edited by Michael J. Shipston

The human innate immunity factor apolipoprotein L-I (APOL1) protects against infection by several protozoan parasites, including *Trypanosoma brucei brucei*. Endocytosis and acidification of high-density lipoprotein–associated APOL1 in trypanosome endosomes leads to eventual lysis of the parasite due to increased plasma membrane cation permeability, followed by colloid-osmotic swelling. It was previously shown that recombinant APOL1 inserts into planar lipid bilayers at acidic pH to form pH-gated nonselective cation channels that are opened upon pH neutralization. This corresponds to the pH changes encountered during endocytic recycling, suggesting APOL1 forms a cytotoxic cation channel in the parasite plasma membrane. Currently, the mechanism and domains required for channel formation have yet to be elucidated, although a predicted helix-loop-helix (H-L-H) was suggested to form pores by virtue of its similarity to bacterial pore-forming colicins. Here, we compare recombinant human and baboon APOL1 orthologs, along with interspecies chimeras and individual amino acid substitutions, to identify regions required for channel formation and pH gating in planar lipid bilayers. We found that whereas neutralization of glutamates within the H-L-H may be important for pH-dependent channel formation, there was no evidence of H-L-H involvement in either pH gating or ion selectivity. In contrast, we found two residues in the C-terminal domain, tyrosine 351 and glutamate 355, that influence pH gating properties, as well as a single residue, aspartate 348, that determines both cation selectivity and pH gating. These data point to the predicted transmembrane region closest to the APOL1 C terminus as the pore-lining segment of this novel channel-forming protein.

Apolipoprotein L-I (APOL1) is a channel-forming innate immune factor that circulates on serum high-density lipoproteins (1). The most well-studied role of APOL1 is in protection against African trypanosome infection. APOL1, APOA1 (apolipoprotein A-1), Hpr (haptoglobin-related protein), and IgM are components of serum trypanosome lytic factors (TLFs), with APOL1 constituting the cytolytic component (2, 3). TLFs protect against infection by several trypanosome parasites, including *Trypanosoma congolense* and *Trypanosoma brucei* (1, 4, 5), as well as more distantly related *Leishmania* parasites (6). However, globally common human APOL1 variants cannot protect against APOL1-resistant *T. brucei gambiense* and *T. brucei rhodesiense*, the parasite species responsible for human African trypanosomiasis. In primates, the APOL1 gene is evolving rapidly, and variants exist with broader trypanolytic potential. For example, baboon APOL1 orthologs kill both human-infective subspecies *T. brucei rhodesiense* and *T. brucei gambiense*, whereas a human APOL1 variant termed G2 protects against *T. brucei rhodesiense* infection (7, 8). A second human APOL1 variant termed G1 was associated with reduced severe disease caused by *T. brucei gambiense* (9). This protection comes at a cost, however, as both the APOL1 G1 and G2 variants cause kidney disease with an etiology based on podocyte injury (10, 11).

Following endocytic uptake of high-density lipoprotein–associated APOL1 into acidic parasite endosomes, African trypanosomes undergo colloid-osmotic swelling and eventual lysis due to an increased plasma membrane cation permeability, which is proposed to result from APOL1 recycling to the plasma membrane, where it forms nonselective cation channels (12, 13). In agreement with this model, cation channel formation by recombinant human APOL1 requires acidic pH (as in endosomes), whereas channel opening requires subsequent pH neutralization (as in recycling to the plasma membrane) (14, 15). APOL1 G1 and G2 expression in podocytes and immortalized cell lines also causes cytoplasmic swelling, which is proposed to result from dysregulated APOL1 channel activity at the plasma membrane (16, 17).

Despite implications for both trypanosomiasis and kidney disease, the molecular details of channel formation by APOL1 remain poorly understood. APOL1 lacks close homology with any known channel-forming proteins, although analogies are made to bacterial pore-forming toxins. Similar to APOL1, these toxins exist as soluble proteins that undergo a conformational change at acidic pH and associate with lipid bilayers to form membrane pores (18). APOL1 also contains a predicted helix-loop-helix (H-L-H) of putative membrane-spanning helices (residues 177–228), which is analogous to the so-called hydrophobic hairpin of diphtheria toxin translocation domain

This article contains supporting information.

* For correspondence: Russell Thomson, rthomson@genectr.hunter.cuny.edu.
Present address for Charles Schaub: Vanderbilt University, Nashville, Tennessee, USA.

© 2020 Schaub et al. Published under exclusive license by The American Society for Biochemistry and Molecular Biology, Inc.

(DpTx-TD) and pore-forming colicins. The hairpin is buried in the crystal structures of colicin and diphtheria toxins at neutral pH (19, 20), yet can insert into lipid bilayers at acidic pH and is integral to channel formation (21, 22). Indeed, a peptide just encompassing the hairpin of DpTx-TD (helices 8 and 9) forms channels with conductance properties similar to those of the intact DpTx-TD (23).

Based on hairpin homology, and on similarity to the C-terminal domain of pore-forming colicins, it was proposed that residues 60–235 of APOL1 constitute the "pore-forming domain" (24). However, the relevance of the H-L-H to channel formation by APOL1 has not been experimentally tested. Unlike in colicins, there are 170 amino acids C-terminal of the APOL1 H-L-H, including a C-terminal domain (CTD; residues 332-398) that contains a putative transmembrane helix and a leucine zipper domain; the CTD also contains the G1 and G2 amino acid changes responsible for APOL1 variant–associated kidney disease. Truncated APOL1 fragments that lack parts of the CTD cannot form channels and do not kill trypanosomes, suggesting that the CTD may be involved in channel formation (4, 14). However, it remains to be seen whether these deficiencies result simply from misfolding of these protein fragments.

In this study, we exploited a baboon APOL1 ortholog which is different enough from human APOL1 (59% identity) to engender enhanced trypanolytic potential yet similar enough to form functional human-baboon APOL1 chimeras (8). We show that recombinant baboon APOL1 forms conductances in planar lipid bilayers that are less pH-dependent and less cation-selective than those formed by human APOL1. Using interspecies chimeras, as well as single amino acid substitutions, we dissect the contributions of hairpin (H-L-H) and C-terminal domains to channel formation by APOL1. Although our data point to a role of the hairpin in facilitating pH-dependent membrane insertion, we found no evidence for hairpin involvement in selectivity or gating functions. Instead, we demonstrate a central role for the putative transmembrane region of the CTD in these aspects of channel formation.

Results

Differences between the lytic capacities of human and baboon APOL1 have long been established, with baboon APOL1 having the ability to lyse the human-infective subspecies *T. brucei rhodesiense* and *T. brucei gambiense* (7, 8). Whereas C-terminal differences account for lysis of *T. brucei rhodesiense*, the mechanism by which *T. brucei gambiense* is lysed by baboon APOL1 has yet to be identified. To identify potential differences in channel-forming properties between human and baboon APOL1, recombinant APOL1 (rAPOL1) proteins were first purified from *Escherichia coli* as described previously (14, 25). Recombinant human APOL1 (HsAPOL1) and recombinant baboon APOL1 (PhAPOL1) were first tested in 24-h trypanolytic assays. As expected, both proteins killed *T. brucei brucei* 427 *in vitro* (Fig. S1), whereas PhAPOL1 also killed 427-SRA (*T. brucei rhodesiense)* and *T. brucei gambiense,* confirming its enhanced lytic activity (Fig. S2).

Substitution of human-specific glutamate residues into the baboon APOL1 H-L-H increases the pH dependence of channel formation

To assess any differences in channel formation, we compared the ability of HsAPOL1 and PhAPOL1 to form a conductance in the planar lipid bilayers (Fig. 1*A*). As reported previously, HsAPOL1 can only insert into bilayers to form a conductance when exposed to a *cis*-acidic buffer of pH <6.0 (Fig. 1*B*) (14, 15). In contrast, PhAPOL1 began to form a conductance at *cis* pH 7.2, and the rate of formation was substantially increased when the *cis* side was acidified slightly to pH 6.6 (Fig. 1*B*), indicating a relaxed pH dependence. To account for this difference, we focused on an H-L-H motif (residues 177–228), which may be similar to the hydrophobic hairpin of bacterial pore-forming toxins (26). The H-L-H of HsAPOL1 contains two acidic amino acid residues, glutamate 201 and glutamate 213 (Glu-201/Glu-213), which are replaced by the uncharged alanine 187 and glycine 199 (Ala-187/Gly-199) in PhAPOL1 (Fig. 2). We hypothesized that substituting these glutamate residues to match baboon APOL1 (Fig. 2) would result in a gain of function toward channel formation at pH 7.2 (Fig. 3*A*). However, the ability of HsAPOL1 E201A/E213G to form channels was still dependent on acidification, similar to HsAPOL1 (Fig. 3*B*). In contrast, when PhAPOL1 residues alanine 187 and glycine 199 were substituted for glutamate to match the human residues (A187E/G199E), there was a loss of conductance formation at neutral pH 7.2 (Fig. 3*C*), whereas conductance formation at acidic pH was maintained (Fig. 3*D*). Therefore, nonpolar residues in the baboon APOL1 H-L-H allow for channel formation at neutral pH, whereas the mechanisms by which human APOL1 forms channels in a strictly pH-dependent manner remain unclear.

Interspecies differences in the CTD affect pH gating and selectivity

To investigate potential differences in pH gating between human and baboon APOL1, recombinant proteins were subjected to titrations with KOH and HCl in the planar bilayer system (Fig. 4). As shown previously, the conductance formed by HsAPOL1 is minimal after insertion into the bilayer at pH 5.6 but increases 100–500-fold upon pH neutralization (Fig. 4*A*). This increase, which is plotted as a sigmoidal titration curve with a pK_a of around 7 (Fig. 4*C*), is due to the opening of pH-gated channels (14). In contrast, PhAPOL1 formed a relatively large conductance at pH 5.6, and this conductance increased in a nonsigmoidal manner by only 3–5-fold after alkalization to pH 9.2 (Fig. 4, *B* and *C*). To account for this difference, we returned to the diphtheria toxin-like H-L-H region (Fig. 2). However, HsAPOL1 E201A/E213G had pH gating properties nearly identical to those of HsAPOL1, indicating that these residues do not contribute to channel gating (Fig. S3).

As C-terminal deletions of APOL1 have been shown to lose functional activity, we next asked whether differences between the CTD of baboon and human APOL1 could explain the divergence in pH gating. We previously found that replacing the entire human APOL1 CTD (residues 322–398) with the entire baboon APOL1 CTD (residues 313–388) generated a nonfunctional (nontrypanolytic) chimera in a transgenic mouse system

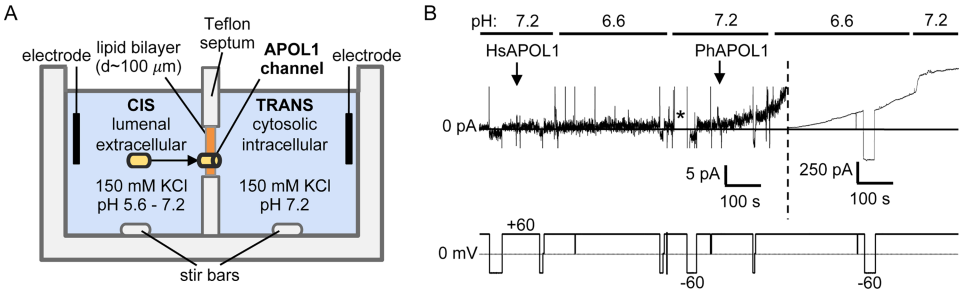

Figure 1. Baboon APOL1 is less pH-dependent than human APOL1. *A*, schematic of the planar lipid bilayer system. *B*, a bilayer was formed in symmetric solutions of chamber buffer, pH 7.2 (see "Materials and methods"). The current was recorded (*top trace*, pA) as the voltage was manipulated (*bottom trace*, mV). 180 ng of HsAPOL1 was added to the *cis* solution, which was then acidified to pH 6.6 with HCl, before being reneutralized with KOH (pH 7.2). During this period, no change in current occurred (except for a brief aberration indicated with an *asterisk*). In contrast, PhAPOL1 addition to the *cis* side of the same bilayer resulted in a gradual conductance increase at pH 7.2 (5-pA scale, *left* of *dashed line*) and a faster rate of increase when the *cis* side was adjusted to pH 6.6 (250-pA scale, *right* of *dashed line*).

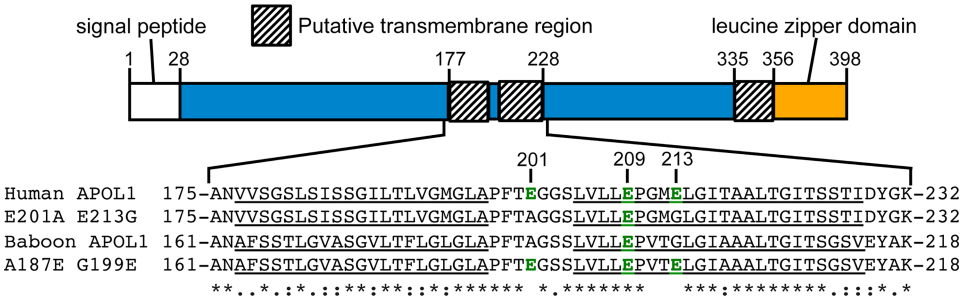

Figure 2. Comparison of the human and baboon APOL1 H-L-H region. *Top*, schematic of full-length APOL1, showing human APOL1 residue positions of the signal peptide (*white box*, not present in recombinant protein) and putative transmembrane regions (*shaded boxes*). Regions of uncharacterized function are shown in *blue*. *Bottom*, amino acid sequence alignment of human APOL1, human APOL1 E201A/E213G, baboon APOL1, and baboon APOL1 A187E/G199E H-L-H regions. Delimiting amino acid residue numbers are shown directly *above* the schematic, whereas notable human-APOL1 residue positions are shown *above* the alignment. Note the presence of negatively charged residues (*green type*), within the otherwise uncharged, putative transmembrane helices (*underlined*). A baboon APOL1 deletion (N-terminal of the alignment) explains the disparate residue numbers of the baboon and human proteins. The alignment was used to identify fully conserved (*), strongly similar (:), or weakly similar (.) amino acid residues.

(8), so instead we opted to use four chimeras (C1–C4) in which different portions of the CTD were exchanged between the human and baboon orthologs (Fig. 5*A*). Whereas pH gating of the C1 chimera (which differs from HsAPOL1 in the leucine zipper domain) was unchanged compared with HsAPOL1, the C2 chimera had altered pH gating with a shift toward the open state at a more acidic pH (Fig. 5*B*). As the C1 and C2 chimeras differ by only four amino acid residues at the C-terminal end of a predicted transmembrane region, we made a third chimera (C3) containing only these baboon-specific residues (Y351G, Y354C, E355Q, and S356L) in a human APOL1 background (Fig. 5*A*). As expected, the titration curve was identical to that of the C2 chimera, indicating that some or all of residues 351 and 354–356 are involved in pH gating (Fig. 5*B*). We then used a fourth chimera (C4; Fig. 5*A*) to ask whether the human residues could reconstitute pH gating when substituted into baboon APOL1. Indeed, the C4 titration curve was shifted to a midway point between the human and baboon APOL1, suggesting partial reconstitution of pH gating (Fig. 5*C*).

To identify which of the four human-specific residues contribute to pH gating, we made individual amino acid substitutions in the HsAPOL1 background (Fig. 5*A*), focusing on the two tyrosines (Tyr-351 and Tyr-354) and the glutamate (Glu-355), as these residues are conceivably proton-titratable within the relevant pH range. The pH gating of HsAPOL1 Y354C was similar to HsAPOL1, whereas the pH gating of APOL1 Y351G and E355Q were significantly altered (Fig. 5*D*). The Y351G substitution caused an approximately one-unit decrease in pK_a, whereas replacing tyrosine with the similarly shaped but untitratable phenylalanine (Y351F) caused no change in the titration curve (Fig. 5*D*). We conclude that Tyr-351 is not the pH sensor, but that it may influence the microenvironment of a pH-gating residue, affecting its apparent pK_a. Conversely, substitution of glutamate 355 for the isosteric but nontitratable glutamine (E355Q) shifted the pK_a nearly one unit toward alkalinity, suggesting that protonation of Glu-355 contributes to normal pH gating of HsAPOL1 (Fig. 5*D*). Interestingly, the effect of Glu-355 on gating was contingent on the presence of tyrosine at position 351, as the C3 chimera (which contains both Y351G and E355Q substitutions) produced a pH titration curve similar to the single Y351G substitution alone (Fig. 5, *B* and *D*). These results suggest that the putative CTD transmembrane region is involved in pH gating of the APOL1 channel.

Having identified separate determinants of channel formation/membrane insertion *versus* pH gating, we next sought to identify the pore-lining region of APOL1. First, we compared the cation *versus* anion selectivity of human and baboon APOL1 by measuring the reversal potential (E_{rev}) in the presence of an increasing *cis*:*trans* KCl gradient (Fig. 6*A*). If the channel pore is nonselective, then KCl will diffuse down its concentration gradient with no net transfer of charge, resulting in E_{rev} = 0. On the other hand, if the channel pore is ideally

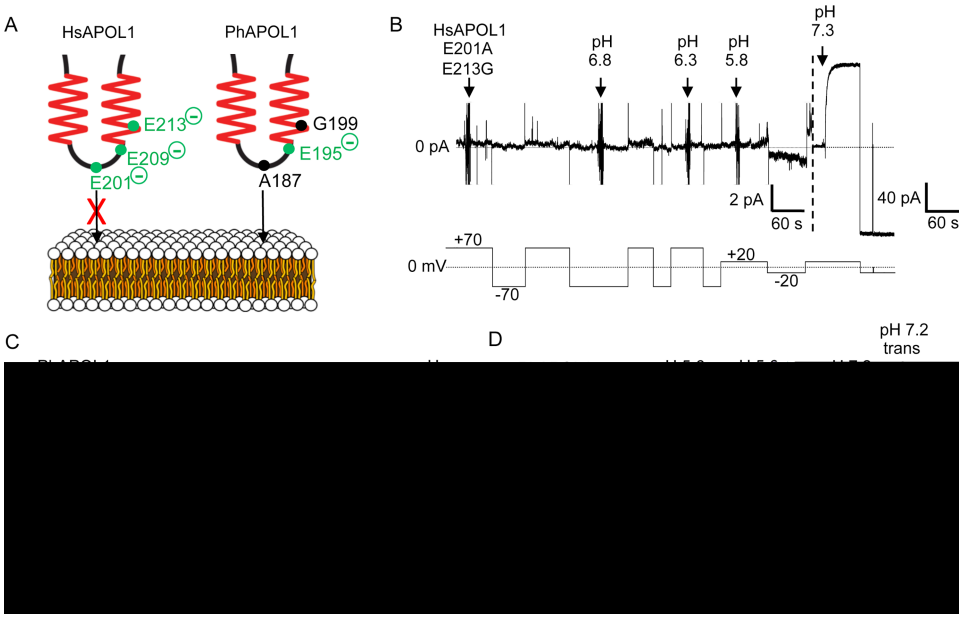

Figure 3. The H-L-H is involved in pH-dependent conductance formation by APOL1. *A*, schematic of human (*left*) and baboon (*right*) APOL1 H-L-H region showing human-specific glutamate residues (*left*), and their baboon-specific counterparts (*right*). At neutral pH, the three charged glutamates of the human H-L-H could impede lipid bilayer insertion of the human H-L-H to a greater extent than the baboon H-L-H, which has only one glutamate in this region (Glu-195). *B–D*, planar lipid bilayers were formed between symmetric solutions of chamber buffer (pH 7.2). Each *panel* represents a separate experiment, during which the experimenter set the voltage (*bottom trace*, mV) as the current was recorded (*top trace*, pA). *B*, a total of 500 ng of HsAPOL1 E201A/E213G was added to the *cis* side, which was then gradually acidified with HCl (2-pA scale, *left side* of *dashed line*). The current did not begin to change until after the pH was brought to 5.8. As expected, subsequent neutralization (pH 7.3) resulted in a large conductance increase due to channel opening (40-pA scale, *right* of *dashed line*). *C*, a total of 160 ng of PhAPOL1 A187E/G199E was added to the *cis* side, which caused no change in current. After perfusion with chamber buffer (pH 7.2) to remove soluble protein, the addition of just 80 ng of PhAPOL1 to the same bilayer resulted in a significant rate of current change at pH 7.2, which was then further increased by acidification to pH 5.6. *D*, 160 ng of PhAPOL1 A187E/G199E was added to the *cis* side, which again did not affect the current at pH 7.2; however, upon acidification to pH 5.6, a rapid increase in the current magnitude was observed, which was visible on the nA scale (*right* of *dashed line*). Similar to PhAPOL1 (see Fig. 4*B*), there was only a 3-fold increase in conductance upon subsequent pH neutralization.

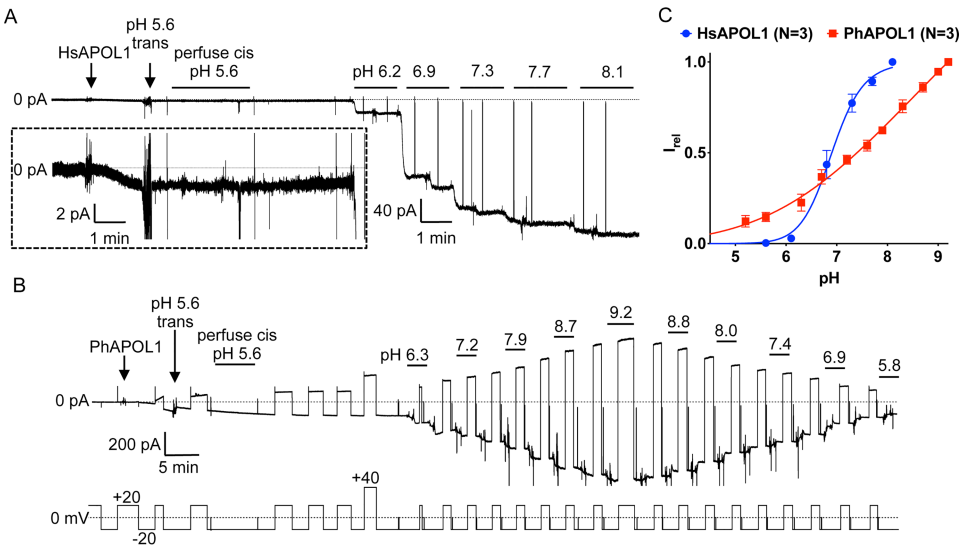

Figure 4. Baboon APOL1 lacks pH gating. *A*, pH dependence of human APOL1. A bilayer was formed between two solutions of chamber buffer with the *cis* side buffered at pH 5.6 and the *trans* at pH 7.2. Except for brief excursions to 0 mV, the voltage was held at −20 mV throughout. The addition of HsAPOL1 resulted in a modest rate of current change (2-pA scale, *inset*) that was halted by acidification of the *trans* side to pH 5.6 with a precalibrated volume of HCl. To remove soluble protein, the *cis* side was perfused with chamber buffer (pH 5.6). The pH was adjusted by alternately adding KOH to first the *cis* and then the *trans* sides to give the symmetric pH values indicated. From pH 5.6 to 8.1, there was a 120-fold increase in conductance. *B*, pH dependence of baboon APOL1. The bilayer was formed as in *A*, except that chamber buffer was supplemented with 5 mM CHES to allow buffering up to pH 9.2. Upon the addition of PhAPOL1, there was a rapid and substantial increase in current at *cis* pH 5.6 (200-pA scale). After *trans* acidification to pH 5.6 and *cis* perfusion (also pH 5.6), the solutions were titrated with KOH as above, resulting in a relatively small 5-fold increase in conductance from pH 5.6 to pH 9.2. The *trans* and *cis* solutions were then back-titrated with HCl. *C*, the current at each value of pH was normalized to the maximal current to obtain the relative current (I_{rel}). Plotted is the average I_{rel} of *n* independent experiments ± S.D. (*error bars*). The data were fit to the Hill equation. In some cases, error bars are smaller than the symbols used to represent data points.

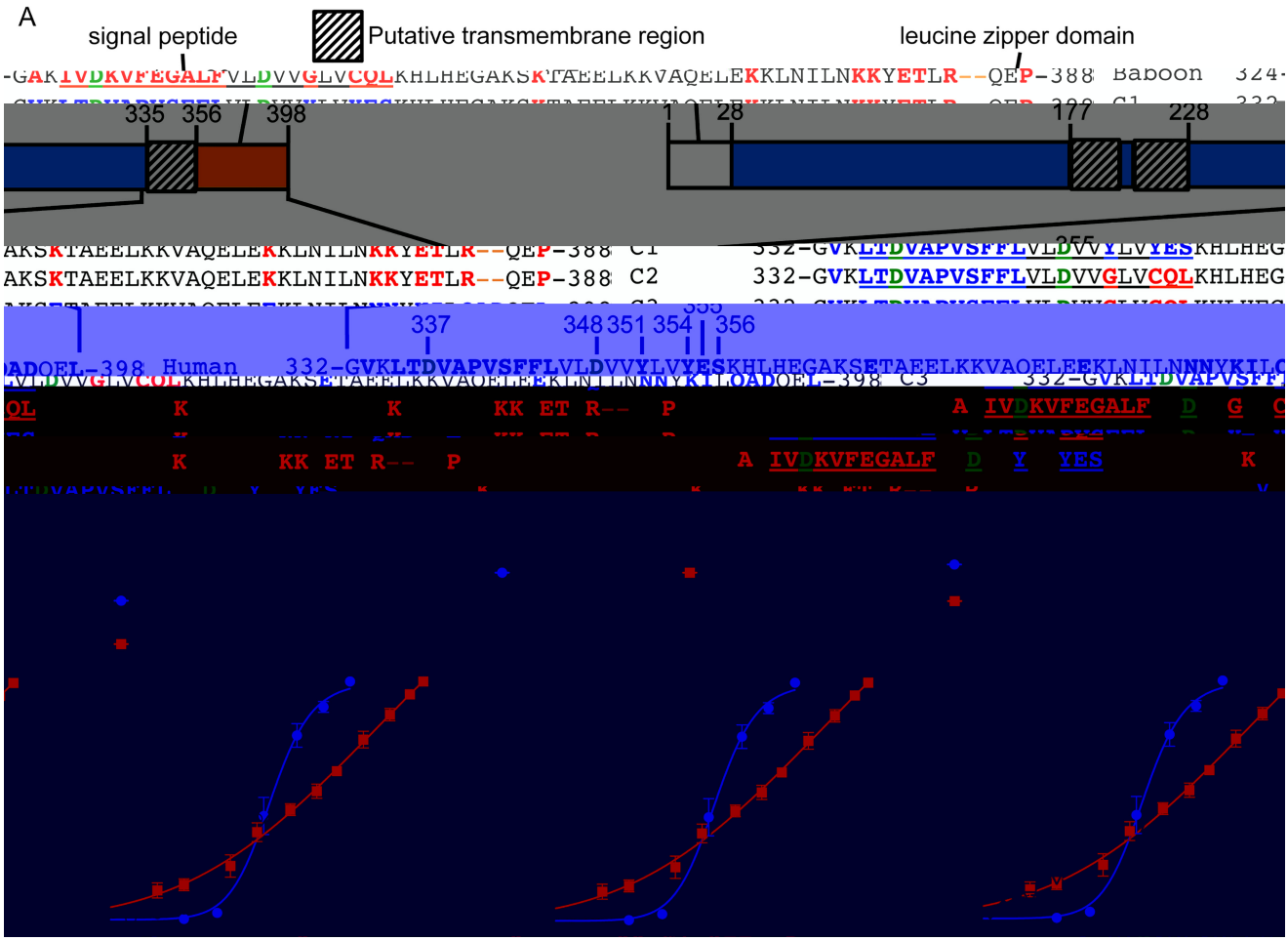

Figure 5. Substitution of CTD residues Tyr-351 and Glu-355 affects pH gating. *A*, amino acid alignment of human, baboon, and chimeric (C1–C4) APOL1 C-terminal domains, with relevant HsAPOL1 residue numbers indicated. A baboon APOL1 deletion (N-terminal of the alignment) explains the disparate residue numbers of the aligned amino acid sequences. The C1–C3 constructs differ from human APOL1 in that the indicated *human-specific* residues (*blue type*) were exchanged for their *baboon-specific* counterparts (*red type*). For example, C3 contains just four baboon-specific residues, and the remainder of the protein is identical to human APOL1, whereas C4 is the inverse chimera of C3; it differs from baboon APOL1 in that just four baboon-specific residues were substituted for their human-specific counterparts. Note that the four residues exchanged in C3 and C4 are situated at the C-terminal end of a putative transmembrane region (*underlined*). Situated in the putative transmembrane region are two conserved aspartate residues, Asp-337 and Asp-348 (*green type*; see "main text" for more details). A Clustal Omega alignment of the human and baboon sequences identified fully conserved (*), strongly similar (:), or weakly similar (.) amino acid residues. *B–D*, a conductance was obtained with each chimera, and pH titration experiments were performed as described in the legend to Fig. 4. The current at each pH value was normalized to the maximal current to obtain the relative current (I_{rel}). Plotted is the average I_{rel} of *n* independent experiments ± S.D. (*error bars*). The data were fit to the Hill equation. In some cases, error bars are smaller than the symbols used to represent data points.

selective for K^+ over Cl^-, then a *cis* negative voltage equal to the Nernst potential must be applied to prevent the net movement of charge (see "Materials and methods"). In agreement with previously published results, HsAPOL1 was ideally cation-selective at pH 7.2 (Fig. 6*B*). Interestingly, we found that PhAPOL1 was not ideally cation-selective at this pH, indicating potential inter-ortholog differences in the pore-lining region (Fig. 6*B*). To identify molecular determinants of this difference, we tested the selectivity of the previously purified chimeras and point substitutions (Figs. 2 and 5*A*). Amino acid changes in the H-L-H, either HsAPOL1 E201A/E213G or PhAPOL1 A187E/G199E, had no effect on selectivity (Fig. 6*B*), and the C-terminal chimeras C1 and C2 were still ideally cation-selective (Fig. 6*C*). However, the inverse chimera on the baboon APOL1 backbone (C4) showed a shift toward ideal cation selectivity (Fig. 6*C*), suggesting that the putative CTD transmembrane region influences cation selectivity of the channel.

CTD residue Asp-348 governs selectivity and pH gating of the APOL1 channel

Upon inspection of the putative CTD transmembrane (residues 335–356), we identified two acidic residues, Asp-337 and Asp-348, that could attract cations to the pore and repel anions when in the unprotonated/negatively charged state at neutral pH (Fig. 5*A*). If so, we reasoned that the permeability ratio of cations to anions would decrease with decreasing pH (as negatively charged side chains become protonated and neutralized). Indeed, when HsAPOL1 was tested in planar lipid bilayers, there was a loss in relative cation permeability as the *cis* chamber was titrated from pH 7.2 to pH 5.6 and a further loss when the pH was dropped to 5.4 (Fig. 7*A*). Under the reverse condition of *cis* pH 7.2, *trans* pH 5.6, APOL1 maintained its ideal cation selectivity (Fig. 7*A*). These results implicate Asp-337 and Asp-348 as possible determinants of APOL1 selectivity.

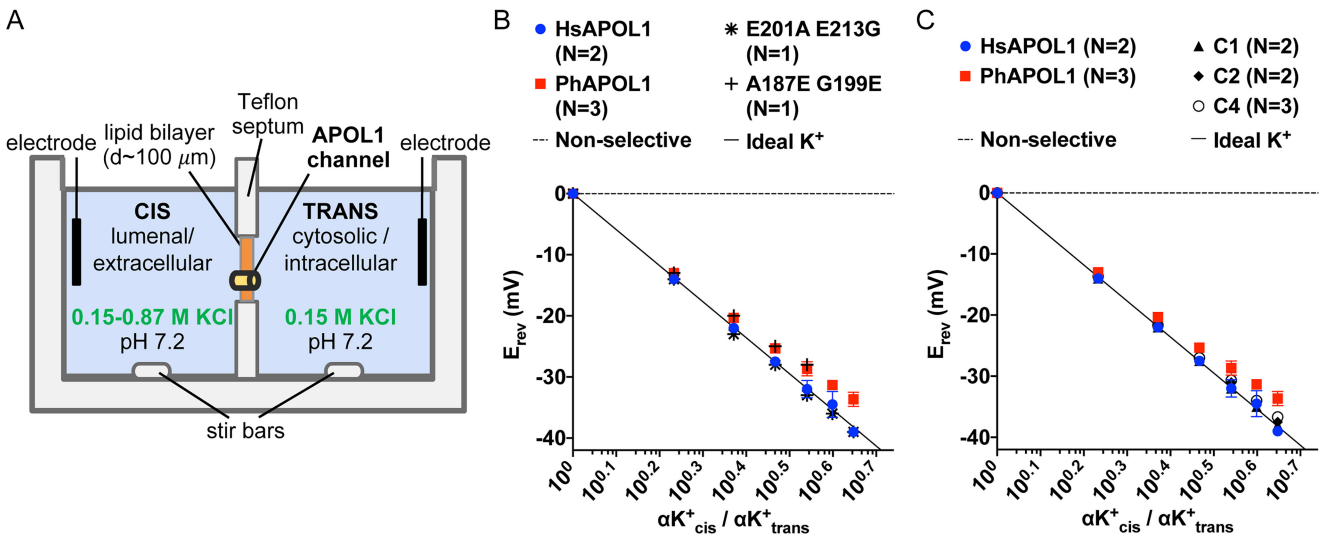

Figure 6. Cation *versus* anion selectivity of human, baboon, and chimeric APOL1. *A*, planar lipid bilayer setup. *B*, a conductance was obtained with APOL1 variants or chimeras as described in the legend to Fig. 4. The *cis* side was then perfused with pH 5.6 buffer and then adjusted to pH 7.2 with KOH. The reversal potential (the voltage at the current registered zero, E_{rev}) was then determined before and after successive additions of 50 μl of 3 M KCl to the *cis* side. *B* and *C*, plotted are average E_{rev} from *N* independent experiments ± S.D. (*error bars*) *versus* the *cis*/*trans* K^+ activity gradient ($\alpha K^+_{cis}/\alpha K^+_{trans}$, K^+ activity was taken as equal to KCl activity; see "Materials and methods"). In some cases, error bars are smaller than the data points. In all cases, electrode offsets were <1 mV. The ideal potassium-selective line is defined by the Nernst potential ($E_{rev} = 59 \times \log_{10}[\alpha K^+_{cis}/\alpha K^+_{trans}]$).

To test this possibility directly, we made individual substitutions of Asp-337 and Asp-348 for the isosteric but uncharged asparagine. The recombinant proteins were then subjected to *in vitro* trypanolytic assays and incorporated into planar lipid bilayers. APOL1 D337N retained lytic activity similar to that of HsAPOL1 (Fig. S4*A*), and there was no significant effect of the D337N substitution on channel formation or pH gating in the planar lipid bilayer system (Fig. 7*B*). Conversely, APOL1 D348N was unable to lyse *T. brucei brucei* 427 at concentrations nearly 8-fold higher than the LD_{50} of HsAPOL1 (Fig. S4*A*). In addition, we found that although APOL1 D348N could insert into lipid bilayers to form a minor conductance at acidic pH, there was little conductance increase (~5-fold) upon pH neutralization when compared directly with HsAPOL1 in the same lipid bilayer (Fig. 7*C*). Thus, it is feasible that Asp-348 acts as a second pH-gating residue along with the Glu-355 residue identified earlier (Fig. 5, *A* and *D*). To test this possibility, we generated an APOL1 mutant containing both D348N and E355Q substitutions. The double substitution eliminated any appreciable conductance increase upon pH neutralization, suggesting that pH gating depends on protonation of both Glu-355 and Asp-348 residues (Fig. S5*B*).

Finally, we investigated the effect of D337N and D348N substitutions on cation selectivity. Whereas APOL1 D337N remained ideally cation-selective, the D348N substitution resulted in reduced cation selectivity at pH 7.2 (Fig. 7*D*), resembling HsAPOL1 at pH 5.4 (Fig. 7*A*). This result indicates that protonation and accompanying charge neutralization of Asp-348 at acidic pH (when it resembles asparagine) reduces the cation permeability of the APOL1 channel. To test the extent of this influence, we replaced Asp-348 with histidine, which is typically uncharged at neutral pH but becomes positively charged at acidic pH. Like APOL1 D348N, APOL1 D348H was unable to lyse African trypanosomes *in vitro* (Fig. S4*A*). Remarkably, the D348H substitution resulted in almost complete loss of ion selectivity in planar lipid bilayers at pH 7.4, whereas at pH 6.1, the conductance became strongly anion-selective (Fig. 7*E*). Taken together, these results suggest that the pH-dependent charge status of residue 348 dictates both selectivity and pH gating functions of the APOL1 channel.

Discussion

It was previously shown that human APOL1 forms pH-gated channels in planar lipid bilayers and kills African trypanosomes via colloid-osmotic lysis (1, 12, 14). In this paper, we use human-baboon APOL1 chimeras and single-amino acid substitutions to identify key residues and domains affecting channel formation, pH gating, and selectivity. Most significantly, a single residue, aspartate 348, was found to govern pH-dependent channel selectivity and gating functions. Our data indicate that the pore-lining region is constituted, at least in part, by the final predicted transmembrane region (residues 335–356), which is located in the C-terminal domain.

To better discern the mechanism of channel formation by APOL1, we first sought to characterize the channel-forming properties of baboon APOL1, which has increased trypanolytic capabilities compared with its human ortholog (7, 27). Unlike HsAPOL1, PhAPOL1 formed channels in planar lipid bilayers at pH 7.2 (Fig. 1*B*). This was supported by trypanolytic assay results wherein 10 mM ammonium chloride (which neutralizes acidic endosomes/lysosomes) was able to completely block lysis by HsAPOL1, but not PhAPOL1 (Fig. S1). Furthermore, PhAPOL1 was able to form a relatively large conductance at pH 5.6, which was increased only 2–3-fold upon subsequent neutralization to pH 7.2 (Fig. 4, compare *A* with *C*). These gain-of-function properties could help to explain how recombinant baboon APOL1 is able to lyse the human-infective parasite *T. brucei gambiense* (28) (Fig. S2).

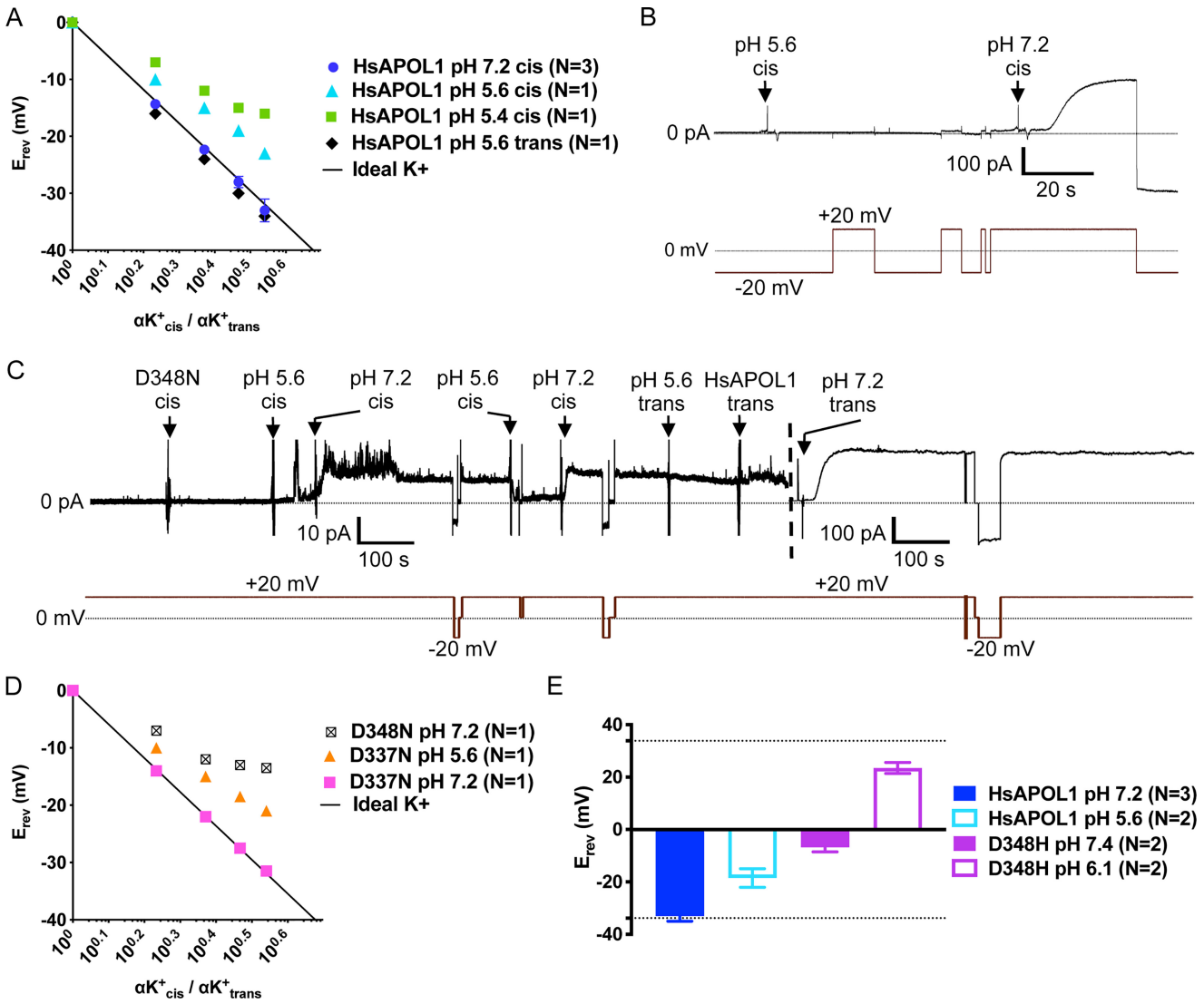

Figure 7. Asp-348 controls cation *versus* anion selectivity of the APOL1 channel. Ion selectivity of HsAPOL1 (*A*) and mutant APOL1 (*D* and *E*) were determined as described in the legend to Fig. 6, except that E_{rev} was obtained at different pH. Data are plotted as mean ± S.D. (*error bars*) of *N* independent experiments. *A*, the conductance formed by HsAPOL1 was ideally cation-selective at pH 7.2 (also see Fig. 6) but became increasingly permeable to anions with decreasing pH. In contrast, acidification of the *trans* pH had no effect on selectivity. In *B* and *C*, the current was recorded (*top trace*) as the voltage was manipulated (*bottom trace*). *B*, before the start of the record, a total of 300 ng of APOL1 D337N was added to the *cis* chamber, which was then acidified with 1 M HCl. Neutralization with 1 M KOH resulted in the typical 200–500-fold conductance increase. *C*, 250 ng of APOL1 D348N was added to the *cis* chamber at pH 7.2, which was then acidified with 1 M HCl to allow for protein insertion into the bilayer. After neutralization of the *cis* chamber with 1 M KOH, there was only about a 5-fold increase in conductance, which was reversed upon *cis* HCl addition. To compare with HsAPOL1 on the same bilayer, the *trans* chamber was then acidified with 1 M HCl, and 250 ng of HsAPOL1 was added to the *trans* side. After *trans* neutralization with 1 M KOH, the expected increase in conductance occurred (*dashed vertical line* indicates change in current scale). *D*, selectivity of APOL1 D337N was comparable with HsAPOL1 at both *cis* pH 7.2 and pH 5.6, whereas the D348N substitution resulted in loss of ideal cation selectivity at *cis* pH 7.2, similar to HsAPOL1 at pH 5.6. *E*, bar graph comparing selectivity of HsAPOL1 and D348H at both acidic and neutral pH with a 3.47-fold *cis*:*trans* KCl activity gradient (see legend to Fig. 6). *Dotted lines*, ideal potassium selectivity (−33 mV) and ideal chloride selectivity (+33 mV) as defined by the Nernst potential.

Having defined key differences in channel formation, gating, and ion selectivity between full-length human and baboon APOL1 orthologs, we then focused on the predicted H-L-H (residues 177–228) as a potential pore-lining region (Fig. 2), due to similarity with the hydrophobic hairpin/H-L-H of the pore-forming colicins and diphtheria toxin (29, 30). However, we were unsuccessful in modulating the ion selectivity of either human or baboon APOL1 by exchanging charged glutamate residues of the H-L-H between human and baboon APOL1 backgrounds (Fig. 6*B*). This is in contrast to diphtheria toxin, wherein substitution of H-L-H glutamates for uncharged glutamines affected single-channel conductance or both selectivity and conductance (pore-forming colicins lack charged residues within the H-L-H) (26). Interestingly, H-L-H substitutions A187E/G199E in the PhAPOL1 background did prevent channel formation at neutral pH, suggesting that negatively charged H-L-H residues must be protonated prior to membrane insertion (Fig. 3, *C* and *D*). The H-L-H may therefore serve as a membrane anchor, allowing for pH-dependent membrane insertion, with the *trans* pH 7.2 "trapping" one or more of the glutamates on the *trans* side (31) (Fig. 3*A*). However, the reverse substitution in the human APOL1 background (E201A/E213G) does not allow channel formation at neutral pH (Fig. 3*B*), indicating that another region

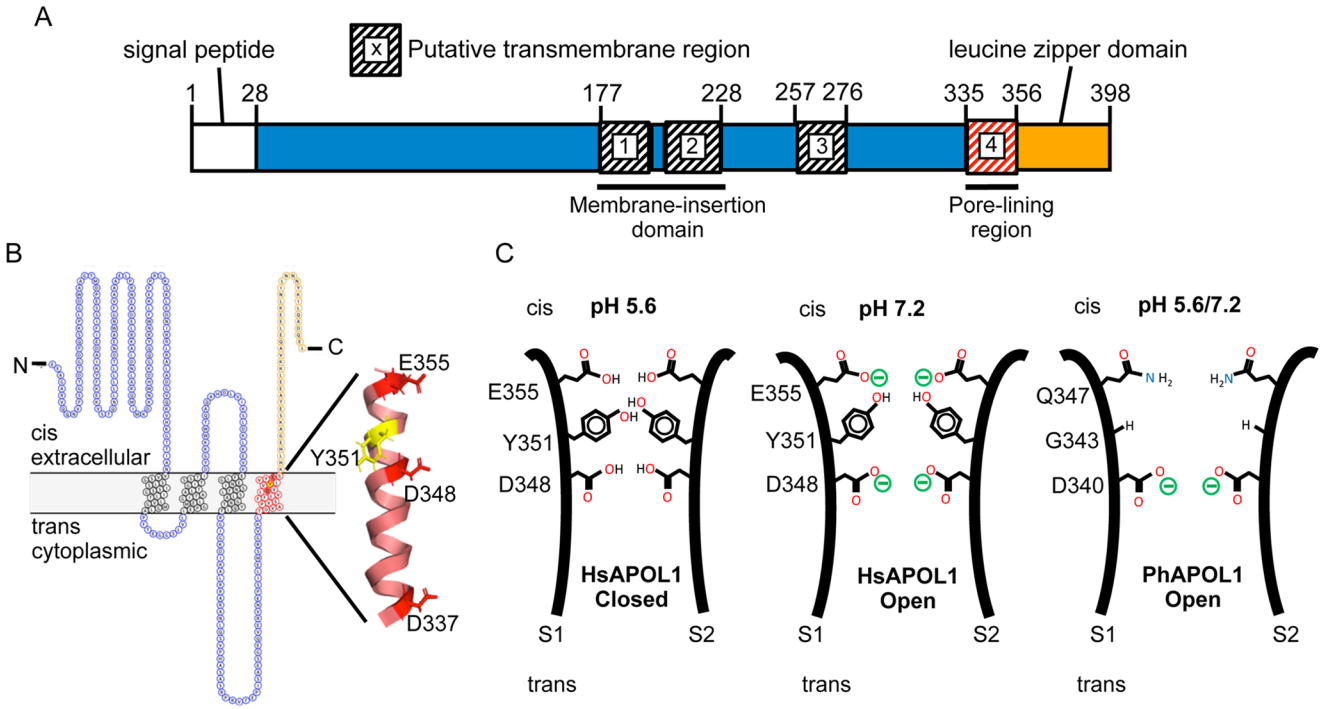

Figure 8. Modeling the domains and pore-lining region of the APOL1 channel. *A*, domain structure. The H-L-H encompasses a hairpin of two transmembrane helices (residues 177–228), which is likely responsible for membrane insertion. Our data suggest that a third transmembrane is situated between the H-L-H and the pore-lining region (residues 335–356), such that Glu-355 may be titrated by changes in *cis* pH. The leucine zipper domain (residues 357–398) may mediate interaction between APOL1 subunits and contains the binding site for the SRA protein of *T. brucei rhodesiense*. *B*, topology model. The *cis* side is equivalent to the extracellular side of the plasma membrane (42). The pore-lining region, shown in *red* (residues 335–356), is modeled as a transmembrane α-helix with the three acidic residues (Asp-337, Asp-348, and Glu-355) and tyrosine 351 aligned along the pore-lining face (43). *C*, speculative model of the pore. In this cross-section, the pore-lining region of two APOL1 subunits (S1 and S2) are brought into apposition via the C-terminal leucine zipper domain. The protonation status of Asp-348 determines pH gating and selectivity of the channel, with the Tyr-351 and Glu-355 pair having an accessory role in pH gating. Tyr-351 sterically blocks the channel in the closed state (pH 5.6), but channel opening is achieved by deprotonation of Glu-355 upon pH neutralization (pH 7.2). This exposes Asp-348 to the *cis* solution, allowing for its deprotonation and the conductance of cations through the channel. PhAPOL1 lacks Tyr-351 and Glu-355 equivalents (replaced by Gly-343 and Gln-347, respectively), and channel opening is less strictly dependent on pH.

works in conjunction with the H-L-H for pH-dependent channel formation to occur.

Unlike the channel-forming domains of bacterial pore-forming toxins, APOL1 contains some 170 amino acids C-terminal to the H-L-H (32). This includes a C-terminal putative leucine zipper domain, which was previously identified as the binding site for the serum resistance–associated protein (SRA) of *T. brucei rhodesiense* (residues 365–398; Fig. 5*A*). Considering the baboon APOL1 leucine zipper domain has a pI of ~8.8, compared with ~4.8 for humans, it is feasible that charge neutralization of this region is also necessary for channel formation (8). Additionally, truncation of the C-terminal leucine zipper domain by 10 or more amino acids abolished trypanolytic activity and was associated with loss of channel-forming ability (4, 14, 33). We therefore refocused on the APOL1 CTD in our search for the prospective pore-lining region (Fig. 5*A*). Using C-terminal chimeras of human and baboon APOL1, we traced differences in pH gating (Fig. 5) and ion selectivity (Fig. 6) to the putative transmembrane region (human APOL1 residues 335–356) of the CTD, which we now postulate to be a pore-lining α-helix (Fig. 8). This region contains two negatively charged aspartate residues, one of which, aspartate 348 (conserved in human and baboon APOL1), was crucially important to the pH-dependent conductance of cations through the channel. The D348N substitution was associated with reduced overall conductance compared with HsAPOL1 (Fig. 7*C*) as well as decreased cation selectivity at neutral pH (Fig. 7*D*), similar to HsAPOL1 at pH 5.4 (Fig. 7*A*). Substitution for histidine (D348H) reduced cation selectivity still further at neutral pH and actually reversed selectivity from cations to anions at acidic pH (Fig. 7*E*). In contrast, substitution of a second aspartate (D337N) within the same putative transmembrane region had no effect on either the pH-dependent conductance properties (Fig. 7*B*) or charge selectivity (Fig. 7*D*). Together, these results suggest that cation selectivity of the APOL1 channel is electrostatic in nature and dependent to a large extent on the protonation status of a single residue, aspartate 348.

Within the C-terminal domain, we also identified two residues, Tyr-351 and Glu-355, that are involved in pH gating (Fig. 5). Whereas Glu-355 may be directly involved in pH sensing, our data indicate that a bulky hydrophobic residue at position 351 impacts the apparent pK_a of a nearby pH sensor, which is not Glu-355. The most promising candidate is Asp-348, as the D348N substitution was associated with minimal channel opening after neutralization (Fig. 7*C*). Thus, the protonation status of Asp-348 likely governs both pH gating and cation selectivity of the APOL1 channel, with Glu-355 having an additional role in pH sensing. In support of this notion, channel opening was all but eliminated by the double substitution D348N/E355Q (Fig. S5*B*).

Although we have not directly addressed the number of transmembrane domains of the APOL1 channel, it is currently predicted that APOL1 transverses the membrane three times, with aspartate-348 part of the third transmembrane domain (7). However, if we accept that the H-L-H of APOL1 contains the first two transmembrane domains (19, 21), then a three-transmembrane model would result in one of the pH-sensing residues, Glu-355, being located on the *trans* side of the membrane and therefore unable to respond to changes in *cis* pH (Fig. S6*A*). However, gating of APOL1 E355Q shows diminished dependence on *cis* pH compared with HsAPOL1, indicating that Glu-355 is located on the *cis* side of the bilayer (Fig. S6, *B* and *C*). At least two alternative possibilities must therefore be considered: 1) Asp-348 is part of a pore loop, and not an actual transmembrane domain, or 2) there is an as yet unidentified transmembrane domain that exists between residues 228 and 335 (*i.e.* within the previously named "membrane-addressing domain" (24)) such that Glu-355 is oriented on the *cis* side of a fourth transmembrane domain (Fig. 8, *A* and *B*). In support of this idea, TMpred-4 software identified a weak transmembrane region spanning residues 257–276 (Fig. S7), which becomes stronger when negatively charged residues are replaced with their uncharged carboximide derivatives to simulate the low pH (protonated) state (Fig. S8). Furthermore, a naturally occurring substitution (N264K) in this region significantly diminished its predicted transmembrane propensity and abrogated both trypanolytic and channel-forming activity (Figs. S7 and S9). The presence of a pore loop also seems unlikely, as these are typically flanked by transmembrane helices (35), which are not apparent in the case of APOL1.

Overall, our data suggest a relatively narrow APOL1 pore with Asp-348 located near the center of its longitudinal axis, such that in the closed channel state, Asp-348 is shielded from the bulk *cis* solution by a constriction of the pore provided by Tyr-351. We propose a leucine zipper dimer model, wherein the deprotonation of Glu-355 at neutral *cis* pH helps to overcome the constriction of the pore imposed by Tyr-351 residues of adjacent subunits, perhaps due to intersubunit electrostatic repulsion between Glu-355 residues pushing the tyrosines apart (Fig. 8*C*). This would increase the exposure of Asp-348 to the bulk *cis* solution and allow for its deprotonation at neutral *cis* pH, which would in turn allow for the conductance of cations through the channel, in agreement with the sigmoidal titration curves we observed (Figs. 5 and 8*C*). In support of this, the Y351G mutation removes the steric block applied by Tyr-351 and shifts the titration curve toward acidic pH, because Asp-348 can now more readily access the *cis* milieu. Conversely, APOL1 E355Q is unable to remove the steric block by deprotonation of Glu-355, and the curve is shifted toward basic pH, due to the limited access of Asp-348 to the bulk *cis* solution (Fig. 5D). It should be noted that we were unable to replicate the nonsigmoidal pH dependence of baboon APOL1 with any of the chimeras tested, suggesting that additional regulatory sequences may exist within the unexamined N-terminal half of the pore-lining region.

Our findings agree with previously published reports that APOL1 forms a cation-selective conductance after the pH is shifted from first acidic (pH 5.5–6.0) to neutral pH, in both planar lipid bilayers and lipid vesicles (14, 15). However, there are conflicting data on the selectivity of APOL1 at acidic pH. Utilizing TLF purified from human plasma, Molina-Portela *et al.* (13) found APOL1 to be nonideally cation-selective in planar lipid bilayers, with a pK^+/pCl^- of 4.7 at *cis* pH 5.5, *trans* pH 7.4. This falls between our estimates of pK^+/pCl^- ~2.9 at *cis* pH 5.4 and ~5.1 at *cis* pH 5.6 (Fig. 7*A*), in agreement with our assessment that APOL1 becomes less selective for cations as aspartate 348 becomes more protonated/neutralized. However, when full-length recombinant APOL1 was inserted into the extravesicular side of phospholipid vesicles at either asymmetric pH (pH 5.5 extravesicular, pH 8.0 intravesicular) or symmetric pH (pH 5.0 extra- and intravesicular), a large, anion-selective conductance was observed when paired with the cation carrier valinomycin (15). Conversely, in planar lipid bilayers, we have only ever observed a relatively small HsAPOL1-induced conductance at asymmetric pH (pH 5.4 *cis* and pH 7.4 *trans*), which was determined in this paper to be nonideally cation-selective (Fig. 7*A*). We conclude that the anion-selective conductance observed by Bruno *et al.* (15) is likely due to a separate molecular species (such as a non-channel-forming APOL1 conformation), which may manifest due to the very low-ionic strength conditions used or the membrane curvature in the vesicle system (34). However, the authors also observed a small acid-dependent cation conductance when rAPOL1 was paired with the chloride carrier Cl1, specifically when rAPOL1 was added under pH 5.0 extravesicular and pH 8.0 intravesicular conditions. This cation conductance was also amplified by neutralization of extravesicular pH, similar to our observations using planar lipid bilayers. Therefore, it appears that formation of the APOL1 cation channel state depends on a neutral *trans*/intravesicular pH to "trap" acidic APOL1 residues in a charged state.

The findings in this paper also shed light on the mechanism of trypanosome lysis by APOL1. It has long been understood that cytoplasmic swelling follows cation flux across the plasma membrane when trypanosomes are treated with human serum (12). This effect can be delayed by adding sucrose to the growth media to prevent osmotic swelling or if either Na^+ ions or Cl^- ions are replaced with the larger ions tetramethylammonium$^+$ or gluconate$^-$, respectively (12, 13). These data support a model in which APOL1 forms cell-surface channels after insertion into the endosome membrane (13). Another group has suggested that APOL1 forms pores in the lysosomal membrane, causing lysosomal swelling and eventual parasite death, or that lysis results from mitochondrial membrane disruption due to the formation of nonselective APOL1 megapores in the outer mitochondrial membrane (24, 36). With regard to the latter, we have never observed anything other than the cation-selective, pH-gated properties described herein. Although APOL1 could possibly collaborate with other trypanosome proteins to form a megapore, it would remain to be explained how the loss-of-function D348N and D348H substitutions might affect this process. Rather, we show that APOL1 D348N and D348H substitutions dramatically reduce APOL1 cation channel conductance (Fig. 7 (*C–E*) and Fig. S5) while eliminating trypanosome killing (Fig. S4). These data also suggest that the residual conductance observed at acidic pH could not explain trypanosome

lysis if it manifested in the lysosomal membrane, as both HsAPOL1 and the loss-of-function D348N/H mutants were competent in this regard (Fig. 7*C* and Fig. S5). Instead, our data further support the notion that endocytic recycling of APOL1 drives lysis of trypanosomes via the pH-dependent opening of APOL1 cation channels in the parasite plasma membrane. Intriguingly, Giovinazzo *et al.* (17) recently reported that induction of human cell swelling and lysis by APOL1 renal risk variants depends on a nonselective cation influx at the plasma membrane. We anticipate that the mutants described herein will allow us to further investigate the precise role of APOL1 cation channels in trypanolysis, as well as the potential role of APOL1 cation channel formation in the development of cytotoxicity caused by APOL1 renal risk variants.

Materials and methods

PCR mutagenesis and bacterial production of APOL1

We used as our human APOL1 coding sequence (accession number O14791) the most globally prevalent variant (Lys-150, Ile-228, Lys-255 (37)). An N-terminally His_6-tagged version of the mature protein, termed as "HsAPOL1" (residues 28–398), was produced by *E. coli* from the pNIC-28 expression vector (Addgene) as described previously (14, 25). The corresponding baboon APOL1 coding sequence was previously obtained from *Papio hamadryas* liver (accession number C9WF17 (8)). The mature protein fragment encoding residues 28–388, termed in this paper as "PhAPOL1", was similarly produced in *E. coli* with an N-terminal His tag. Nucleotide sequences encoding APOL1 chimeras 1 and 2 were generated previously and inserted into pNIC28 (8). All other substitutions and chimeras were generated by site-directed mutagenesis, under standard conditions (QuikChange II, Agilent Technologies).

APOL1 protein purification

Recombinant His-tagged APOL1 was produced as insoluble inclusion bodies in *E. coli* (Bl21-DE3 RIPL, Agilent Technologies) and purified as described previously (14, 25), except for the following modifications. Bacterial pellets were first resuspended and then sonicated in lysis buffer (50 mM Tris-HCl, pH 8.0, 1 mM EDTA), and then 100 μg/ml lysozyme, 5 μg/ml DNase I, and 5 μg/ml RNase I were added. The suspension was stirred for 30 min at room temperature (RT), and then 0.5% (w/v) sodium deoxycholate (made fresh) and 0.5% Triton X-100 (Surfact-AMPS, Pierce) were added, together with 3.5 mM $MgCl_2$ and 2.5 mM $CaCl_2$ to stimulate nuclease activity. After an additional 30 min of stirring at RT, the suspension was sedimented at 26,000 × *g*, resuspended in 1% Triton X-100 and 100 mM NaCl in lysis buffer, and then stirred for an additional 30 min at RT. After further washes with 100 mM NaCl in lysis buffer, followed by 20% (v/v) lysis buffer in water, the pellet was then solubilized in 2% zwittergent 3-14 (Calbiochem) and purified by nickel chelate chromatography, followed by size-exclusion chromatography as detailed previously. The purified protein still dissolved in size-exclusion chromatography buffer (50 mM Tris-HCl, pH 8.5, 150 mM NaCl, 0.05% dodecyl maltoside) was flash-frozen on dry ice in small aliquots (<0.1 ml).

24-h trypanolytic killing assay

Human serum–sensitive Lister-427–derived *T. brucei* 427 were cultured in HMI-9 medium (38). Recombinant APOL1 proteins were serially diluted in HMI-9 medium and then combined with 5×10^5 trypanosomes/ml in triplicate wells of a 96-well plate. The plate was incubated for 20 h at 37 °C (5% CO_2), and then viability was determined using a 4-h alamarBlue assay (Invitrogen) as described by the manufacturer. Data were analyzed and graphed using Prism 8 software by GraphPad.

Planar lipid bilayers

Soybean phospholipids (asolectin/lecithin type IIS from Sigma) were prepared by the method of Kagawa and Racker (39). Planar lipid bilayers were formed essentially as described by Qiu *et al.* (40). Briefly, asolectin and cholesterol (Sigma, C8667) were dissolved together in pentane at concentrations of 1.5 and 0.5% (w/v), respectively. Bilayers were formed across a ~100-μm hole in a Teflon partition separating two 1-ml chambers. The partition was pretreated with 3% (v/v) squalene (Sigma, S3626) in petroleum ether. Unless otherwise stated, chamber buffer (5 mM potassium succinate, 5 mM K-HEPES, 150 mM KCl, 5 mM $CaCl_2$, and 0.5 mM EDTA, pH 7.2) was then added to each side, and 20 μl of the asolectin/cholesterol solution was layered on top. Salt bridges made of 3% (w/v) agar and 3 M KCl connected Ag/AgCl electrodes to the solutions in both compartments. The solvent was allowed to evaporate, and then lipid bilayers were formed by alternately raising the level of each solution above the hole using syringes connected to each side. Lipid bilayer formation was detected as a rapid increase in system capacitance upon raising the solution above the hole. If not observed, the solution levels on each side were alternately lowered and then raised again until a stable bilayer was formed. Each chamber could be stirred by magnetic fleas, allowing for pH adjustment with the addition of precalibrated volumes of 0.5 M HCl or KOH. The *cis* chamber was defined as the side to which protein was added. The voltage was maintained by the BC-535C bilayer clamp (Warner Instruments), and the current output was passed through a low-pass eight-pole Bessel filter (Warner Instruments) at 10 Hz. The voltage of the *cis* side is reported relative to the *trans*. Recording of the current and voltage was done with IGOR NIDAQ Tools MX 1.0 and IGOR software (WaveMetrics) using the National Instruments analog-to-digital converter (NI USB-6211).

Cation *versus* anion selectivity was assessed by measuring the reversal potential of the macroscopic conductance in the presence of varying *cis*:*trans* KCl gradients. The reversal potential (E_{rev}) was determined by adjusting the voltage until the current read zero. The value of E_{rev} in the case of ideal potassium selectivity was calculated using the Nernst potential,

$$E_{rev} = -59\,mV \times \log_{10}\left[\alpha K^{+}{}_{cis}/\alpha K^{+}{}_{trans}\right] \qquad \text{(Eq. 1)}$$

where αK^+ is the potassium$^+$ activity (taken as equal to the KCl activity) (41).

Data availability

All relevant data are contained in the article or in the supporting information.

Acknowledgments—We thank Dr. Alan Finkelstein (Albert Einstein College of Medicine, New York, NY, USA) for generously providing equipment and advice and Dr. Joe Giovinazzo (University of Colorado, Denver, CO, USA) for helpful discussions. We also thank Dr. Jyoti Pant (Hunter College, CUNY) and Alisha Racho-Jansen, MA (Hunter College, CUNY) for constructive critiques of the manuscript.

Author contributions—C. S., J. R., and R. T. conceptualization; C. S., J. V., P. L., N. T., G. L., and R. T. resources; C. S., J. V., P. L., and R. T. formal analysis; C. S., J. R., and R. T. supervision; C. S., J. V., P. L., N. T., G. L., and R. T. investigation; C. S., J. R. and R. T.; C. S. and R. T. methodology; C. S. and R. T. writing-original draft; J. R. funding acquisition; J. R. project administration; J. R and R. T. writing-review and editing.

Funding and additional information—This work was supported by National Science Foundation Grant IOS-1249166 (to J. R.).

Conflict of interest—The authors declare that they have no conflicts of interest with the contents of this article.

Abbreviations—The abbreviations used are: APOL1, apolipoprotein L-I; TLF, trypanosome lytic factor; H-L-H, helix-loop-helix; DpTx-TD, diphtheria toxin translocation domain; CTD, C-terminal domain; SRA, serum resistance–associated protein; RT, room temperature; CHES 2-(cyclohexylamino)ethanesulfonic acid.

References

1. Vanhamme, L., Paturiaux-Hanocq, F., Poelvoorde, P., Nolan, D. P., Lins, L., Van Den Abbeele, J., Pays, A., Tebabi, P., Van Xong, H., Jacquet, A., Moguilevsky, N., Dieu, M., Kane, J. P., De Baetselier, P., Brasseur, R., *et al.* (2003) Apolipoprotein L-I is the trypanosome lytic factor of human serum. *Nature* **422,** 83–87 CrossRef Medline
2. Raper, J., Fung, R., Ghiso, J., Nussenzweig, V., and Tomlinson, S. (1999) Characterization of a novel trypanosome lytic factor from human serum. *Infect. Immun.* **67,** 1910–1916 CrossRef Medline
3. Verdi, J., Zipkin, R., Hillman, E., Gertsch, R. A., Pangburn, S. J., Thomson, R., Papavasiliou, N., Sternberg, J., and Raper, J. (2020) Inducible germline IgMs bridge trypanosome lytic factor assembly and parasite recognition. *Cell Host Microbe* **28,** 79–88.e4 CrossRef Medline
4. Molina-Portela, M. P., Samanovic, M., and Raper, J. (2008) Distinct roles of apolipoprotein components within the trypanosome lytic factor complex revealed in a novel transgenic mouse model. *J. Exp. Med.* **205,** 1721–1728 CrossRef Medline
5. Wheeler, R. J. (2017) Use of chiral cell shape to ensure highly directional swimming in trypanosomes. *PLoS Comput. Biol.* **13,** e1005353 CrossRef Medline
6. Samanovic, M., Molina-Portela, M. P., Chessler, A.-D. C., Burleigh, B. A., and Raper, J. (2009) Trypanosome lytic factor, an antimicrobial high-density lipoprotein, ameliorates *Leishmania* infection. *PLoS Pathog.* **5,** e1000276 CrossRef Medline
7. Thomson, R., Genovese, G., Canon, C., Kovacsics, D., Higgins, M. K., Carrington, M., Winkler, C. A., Kopp, J., Rotimi, C., Adeyemo, A., Doumatey, A., Ayodo, G., Alper, S. L., Pollak, M. R., Friedman, D. J., *et al.* (2014) Evolution of the primate trypanolytic factor APOL1. *Proc. Natl. Acad. Sci. U. S. A.* **111,** E2130–E2139 CrossRef Medline
8. Thomson, R., Molina-Portela, P., Mott, H., Carrington, M., and Raper, J. (2009) Hydrodynamic gene delivery of baboon trypanosome lytic factor eliminates both animal and human-infective African trypanosomes. *Proc. Natl. Acad. Sci. U. S. A.* **106,** 19509–19514 CrossRef Medline
9. Cooper, A., Ilboudo, H., Alibu, V. P., Ravel, S., Enyaru, J., Weir, W., Noyes, H., Capewell, P., Camara, M., Milet, J., Jamonneau, V., Camara, O., Matovu, E., Bucheton, B., MacLeod, A., *et al.* (2017) APOL1 renal risk variants have contrasting resistance and susceptibility associations with African trypanosomiasis. *Elife* **6,** e25461 CrossRef Medline
10. Friedman, D. J., and Pollak, M. R. (2016) Apolipoprotein L1 and kidney disease in African Americans. *Trends Endocrinol. Metab.* **27,** 204–215 CrossRef Medline
11. Genovese, G., Friedman, D. J., Ross, M. D., Lecordier, L., Uzureau, P., Freedman, B. I., Bowden, D. W., Langefeld, C. D., Oleksyk, T. K., Uscinski Knob, A. L., Bernhardy, A. J., Hicks, P. J., Nelson, G. W., Vanhollebeke, B., Winkler, C. A., *et al.* (2010) Association of trypanolytic ApoL1 variants with kidney disease in African Americans. *Science* **329,** 841–845 CrossRef Medline
12. Rifkin, M. R. (1984) *Trypanosoma brucei*: biochemical and morphological studies of cytotoxicity caused by normal human serum. *Exp. Parasitol.* **58,** 81–93 CrossRef Medline
13. Molina-Portela, M. D P., Lugli, E. B., Recio-Pinto, E., and Raper, J. (2005) Trypanosome lytic factor, a subclass of high-density lipoprotein, forms cation-selective pores in membranes. *Mol. Biochem. Parasitol.* **144,** 218–226 CrossRef Medline
14. Thomson, R., and Finkelstein, A. (2015) Human trypanolytic factor APOL1 forms pH-gated cation-selective channels in planar lipid bilayers: relevance to trypanosome lysis. *Proc. Natl. Acad. Sci. U. S. A.* **112,** 2894–2899 CrossRef Medline
15. Bruno, J., Pozzi, N., Oliva, J., and Edwards, J. C. (2017) Apolipoprotein L1 confers pH-switchable ion permeability to phospholipid vesicles. *J. Biol. Chem.* **292,** 18344–18353 CrossRef Medline
16. Olabisi, O. A., Zhang, J.-Y., VerPlank, L., Zahler, N., DiBartolo, S., Heneghan, J. F., Schlöndorff, J. S., Suh, J. H., Yan, P., Alper, S. L., Friedman, D. J., and Pollak, M. R. (2016) APOL1 kidney disease risk variants cause cytotoxicity by depleting cellular potassium and inducing stress-activated protein kinases. *Proc. Natl. Acad. Sci. U. S. A.* **113,** 830–837 CrossRef Medline
17. Giovinazzo, J. A., Thomson, R. P., Khalizova, N., Zager, P. J., Malani, N., Rodriguez-Boulan, E., Raper, J., and Schreiner, R. (2020) Apolipoprotein L-1 renal risk variants form active channels at the plasma membrane driving cytotoxicity. *Elife* **9,** e51185 CrossRef Medline
18. Finkelstein, A. (1990) Channels formed in phospholipid bilayer membranes by diphtheria, tetanus, botulinum and anthrax toxin. *J. Physiol. (Paris)* **84,** 188–190 Medline
19. Choe, S., Bennett, M. J., Fujii, G., Curmi, P. M., Kantardjieff, K. A., Collier, R. J., and Eisenberg, D. (1992) The crystal structure of diphtheria toxin. *Nature* **357,** 216–222 CrossRef Medline
20. Zakharov, S. D., and Cramer, W. A. (2002) Colicin crystal structures: pathways and mechanisms for colicin insertion into membranes. *Biochim. Biophys. Acta* **1565,** 333–346 CrossRef Medline
21. Kienker, P. K., Qiu, X., Slatin, S. L., Finkelstein, A., and Jakes, K. S. (1997) Transmembrane insertion of the colicin Ia hydrophobic hairpin. *J. Membr. Biol.* **157,** 27–37 CrossRef Medline
22. Wang, J., and London, E. (2009) The membrane topography of the diphtheria toxin T domain linked to the a chain reveals a transient transmembrane hairpin and potential translocation mechanisms. *Biochemistry* **48,** 10446–10456 CrossRef Medline
23. Silverman, J. A., Mindell, J. A., Finkelstein, A., Shen, W. H., and Collier, R. J. (1994) Mutational analysis of the helical hairpin region of diphtheria toxin transmembrane domain. *J. Biol. Chem.* **269,** 22524–22532 Medline
24. Pérez-Morga, D., Vanhollebeke, B., Paturiaux-Hanocq, F., Nolan, D. P., Lins, L., Homblé, F., Vanhamme, L., Tebabi, P., Pays, A., Poelvoorde, P., Jacquet, A., Brasseur, R., and Pays, E. (2005) Apolipoprotein L-I promotes trypanosome lysis by forming pores in lysosomal membranes. *Science* **309,** 469–472 CrossRef Medline

25. Verdi, J., Schaub, C., Thomson, R., and Raper, J. (2020) All you ever wanted to know about APOL1 and TLFs and did not dare ask. *Methods Mol. Biol.* **2116,** 463–483 CrossRef Medline
26. Mindell, J. A., Silverman, J. A., Collier, R. J., and Finkelstein, A. (1994) Structure-function relationships in diphtheria toxin channels: III. Residues which affect the *cis* pH dependence of channel conductance. *J. Membr. Biol.* **137,** 45–57 CrossRef Medline
27. Kageruka, P., Mangus, E., Bajyana Songa, E., Nantulya, V., Jochems, M., Hamers, R., and Mortelmans, J. (1991) Infectivity of *Trypanosoma* (*Trypanozoon*) *brucei gambiense* for baboons (*Papio hamadryas, Papio papio*). *Ann. Soc. Belg. Med. Trop.* **71,** 39–46 Medline
28. Cooper, A., Capewell, P., Clucas, C., Veitch, N., Weir, W., Thomson, R., Raper, J., and MacLeod, A. (2016) A primate APOL1 variant that kills *Trypanosoma brucei gambiense*. *PLoS Negl. Trop. Dis.* **10,** e0004903 CrossRef Medline
29. Parker, M. W., Pattus, F., Tucker, A. D., and Tsernoglou, D. (1989) Structure of the membrane-pore-forming fragment of colicin A. *Nature* **337,** 93–96 CrossRef Medline
30. Huynh, P. D., Cui, C., Zhan, H., Oh, K. J., Collier, R. J., and Finkelstein, A. (1997) Probing the structure of the diphtheria toxin channel: reactivity in planar lipid bilayer membranes of cysteine-substituted mutant channels with methanethiosulfonate derivatives. *J. Gen. Physiol.* **110,** 229–242 CrossRef Medline
31. Kaul, P., Silverman, J., Shen, W. H., Blanke, S. R., Huynh, P. D., Finkelstein, A., and Collier, R. J. (1996) Roles of Glu 349 and Asp 352 in membrane insertion and translocation by diphtheria toxin. *Protein Sci.* **5,** 687–692 CrossRef Medline
32. Martinez, M. C., Lazdunski, C., and Pattus, F. (1983) Isolation, molecular and functional properties of the C-terminal domain of colicin A. *EMBO J.* **2,** 1501–1507 CrossRef Medline
33. Lecordier, L., Vanhollebeke, B., Poelvoorde, P., Tebabi, P., Paturiaux-Hanocq, F., Andris, F., Lins, L., and Pays, E. (2009) C-terminal mutants of apolipoprotein L-I efficiently kill both *Trypanosoma brucei brucei* and *Trypanosoma brucei rhodesiense*. *PLoS Pathog.* **5,** e1000685 CrossRef Medline
34. Sobko, A. A., Kotova, E. A., Antonenko, Y. N., Zakharov, S. D., and Cramer, W. A. (2004) Effect of lipids with different spontaneous curvature on the channel activity of colicin E1: evidence in favor of a toroidal pore. *FEBS Lett.* **576,** 205–210 CrossRef Medline
35. (2009) Pore-loop channels. In *Encyclopedia of Neuroscience* (Binder, M.D., Hirokawa, N., and Windhorst, U., eds) p. 3183, Springer, Berlin
36. Vanwalleghem, G., Fontaine, F., Lecordier, L., Tebabi, P., Klewe, K., Nolan, D. P., Yamaryo-Botté, Y., Botté, C., Kremer, A., Burkard, G. S., Rassow, J., Roditi, I., Pérez-Morga, D., and Pays, E. (2015) Coupling of lysosomal and mitochondrial membrane permeabilization in trypanolysis by APOL1. *Nat. Commun.* **6,** 8078 CrossRef Medline
37. Lannon, H., Shah, S. S., Dias, L., Blackler, D., Alper, S. L., Pollak, M. R., and Friedman, D. J. (2019) Apolipoprotein L1 (APOL1) risk variant toxicity depends on the haplotype background. *Kidney Int.* **96,** 1303–1307 CrossRef Medline
38. Hirumi, H., and Hirumi, K. (1989) Continuous cultivation of *Trypanosoma brucei* blood stream forms in a medium containing a low concentration of serum protein without feeder cell layers. *J Parasitol* **75,** 985–989 CrossRef Medline
39. Kagawa, Y., and Racker, E. (1971) Partial resolution of the enzymes catalyzing oxidative phosphorylation: XXV. Reconstitution of vesicles catalyzing 32Pi-adenosine triphosphate exchange. *J. Biol. Chem.* **246,** 5477–5487
40. Qiu, X. Q., Jakes, K. S., Kienker, P. K., Finkelstein, A., and Slatin, S. L. (1996) Major transmembrane movement associated with colicin Ia channel gating. *J. Gen. Physiol.* **107,** 313–328 CrossRef Medline
41. Robinson, R. A., and Stokes, R. H. (1965) *Electrolyte Solutions*, 2nd (revised) Ed., pp. 223–252, Butterworths, London
42. Omasits, U., Ahrens, C. H., Müller, S., and Wollscheid, B. (2014) Protter: interactive protein feature visualization and integration with experimental proteomic data. *Bioinformatics* **30,** 884–886 CrossRef Medline
43. DeLano, W. L. (2012) *The PyMOL Molecular Graphics System*, version 1.5.0.1, Schroedinger, LLC, New York